Small-signal Analysis of DC Microgrid and Multi-objective Optimization Segmented Droop Control Suitable for Economic Dispatch

Haiyuan Liu, Yingjie Wang, Min Wang, Yinan Guo, Jiashi Wang, Gang Shen, and Guoqiang Liao

***Abstract*—To obtain a larger controllable range of output/input power of droop-control sources, a multi-objective optimization segmented droop control suitable for economic dispatch for a DC microgrid is proposed. According to the small-signal analysis, the worst point of the stability in the droop-control curve is determined through the analysis of a simplified model with multiple droop-control sources. By considering the worst points of stability as constraints, an elitist non-dominated sorting genetic algorithm is used to search the better turning points of the proposed droop-control curves after obtaining the new rated operation points from the system-layer economic dispatch. Simultaneously, optimization objectives, including the influence of eliminating the line resistance and capacity matching, are considered in the search process. Finally, the simulation results of the DC microgrid simulation model based on RT-Lab are presented to support the stability conclusion and proposed droop control.**

***Index Terms*—Small signal, DC microgrid, droop control, elitist non-dominated sorting genetic algorithm (NSGA-II).**

I. Introduction

With the increasing penetration of renewable energy sources integrated into modern electric power grids, microgrid is considered as a promising new form of grid organization [1]. Compared with an AC microgrid, a DC microgrid offers many obvious advantages such as the use of two wires instead of three, lower control complexity, and shorter energy-conversion chain. Thus, the DC-AC or AC-DC conversion for DC sources is omitted [2], [3]. With large-scale application of DC sources such as photovoltaic (PV) modules, batteries, and light-emitting diodes (LEDs), hotspot for the DC microgrid is rapidly increasing.

A DC microgrid has many functions such as economic dispatch, operation-mode switching, bus-voltage control, and maximum power-point tracking [4]-[8]. Since these functions have different real-time requirements, hierarchical control architecture composed of the system, converter, and user layers is proposed [9]. The system layer realizes economic dispatch that does not require a real-time control, and some intelligent optimization algorithms are usually used to search the optimal rated operation points of the different sources in a fixed period [10]-[14]. These rated operation points are transmitted to the converter layer that realizes real-time coordination among the converters. The real-time coordination is relatively high. Droop control, which is generally used for a non-communication system, is required [15]-[17]. Therefore, when the rated operation points change, we need to address the problem on how a better droop control follows.

In [18], a switching control method between the droop control and constant-voltage/constant-current control is proposed. The method solves the problem that when the droop curve is constant, the operation point of the system excessively varies, and the DC-bus voltage deviates far from the rated value.

However, the constant-voltage/constant-current control results in uncontrollable power. In [3], an additional amount is introduced to the droop-curve equation to shift the droop curve of the converter so that the output voltage of the converter becomes stable. However, the additional amount needs to be coordinated among the converters. Translation strategies of the droop curves with different coordinated control strategies are proposed in [19], [20]. However, these control strategies do not take into account the maximum output/input power limitations of the converter. When the droop curve changes with the operation point change, the effective working range of the droop control is reduced.

If the droop coefficient is changed, stability should be fully considered. The small-signal stability analysis method is usually adopted, e.g., the impedance-matching method [21]. However, this method is very conservative for the parame-

Manuscript received: December 10, 2018; accepted: October 12, 2019. Date of CrossCheck: October 12, 2019. Date of online publication: February 28, 2020.

This work was supported by the National Key R&D Program of China (No. 2016YFC0600906), the National Natural Science Foundation of China (No. U1810124), the Xuzhou Promoting Science and Technology Innovation Projects (No. KC18076) and the Natural Science Foundation of Jiangsu Province (No. BK20160268).

H. Liu and Y. Guo are with the School of Information and Control Engineering, China University of Mining and Technology, Xuzhou 221000, China (e-mail: liu6340@126.com; nanfly@126.com).

Y. Wang (corresponding author), M. Wang, and J. Wang are with the School of Electrical and Power Engineering, China University of Mining and Technology, Xuzhou 221000, China (e-mail: wyj971@126.com; Wm17851145885@163.com; 13913476267@163.com).

G. Shen is with the School of Mechanical Engineering, China University of Mining and Technology, Xuzhou 221000, China (e-mail: shenganghit@163.com).

G. Liao is with CRRC Zhuzhou Locomotive Co., Ltd., Zhuzhou 412001, China (e-mail: 13574289075@qq.com).

DOI: 10.35833/MPCE.2018.000878

ters. Thus, some methods to improve the forbidden zone [22], [23] are put forward. However, the small-signal stability analysis is only applicable near a certain operation point. To analyze the stability in a wider range, the large-signal stability-analysis method is generally used. In [24], stability determination of a DC-DC cascaded system in a larger scope of work is achieved using the mixed-potential theory. In [25] and [26], large-signal analysis is performed to confirm the increased stability of the operation range using an active damper added to the source converter. In [27], the optional range of the droop coefficient under a certain operation condition is achieved using large-signal analysis. In [28], reachability analysis is performed to analyze the effectiveness of the droop-control method in the existence of uncertainties using the state-space model of a DC microgrid. The aforementioned large-signal stability analysis mainly considers two cascaded DC-DC converters. However, the actual system consists of multiple converters. In [29], the DC-DC gyrator model and equivalent processing of droop-control loop are used to simplify the models of various converters and establish the approximate DC microgrid model. On this basis, a nonlinear stability analysis is performed using the bifurcation theory.

In this paper, first, a simplified model with multiple droop-control sources is built, and the worst point of stability in the droop-control curve is determined using a small-signal analysis. Ensuring the stability of this point is considered as a constraint for the optimal selection of the droop curves. Second, to ensure that each converter can work efficiently under droop control, when the rated operation points change or the load changes, a multi-objective optimization segmented droop control is proposed. The optimization objectives, including the influence of eliminating the line resistance and capacity matching, are considered in the search process. Using the elitist non-dominated sorting genetic algorithm (NSGA-II) [29], better turning points are calculated after obtaining the newly rated operation points from the system-layer economic dispatch. The continuous droop control and controllable range of the output/input power are improved in a wider range of operations. Finally, we present the DC microgrid simulation model based on RT-Lab. The simulation results show that the stability analysis and proposed droop control are valid.

II. Modeling and Stability Analysis of a DC Microgrid

A typical DC microgrid system is shown in Fig. 1.

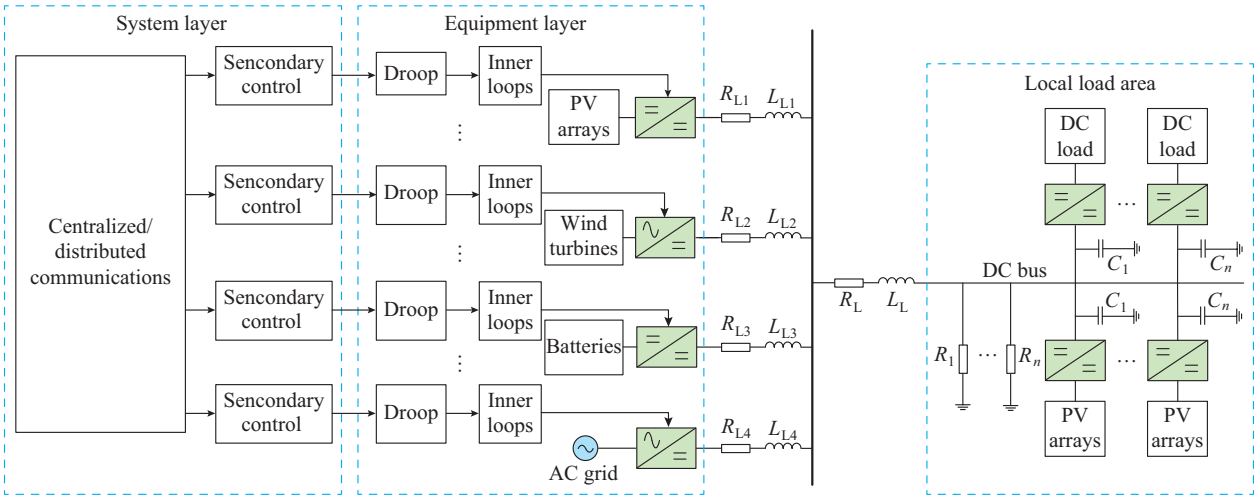

Fig. 1. Schematic diagram of studied DC microgrid.

In [3], [19], and [20], the traditional droop-curve translation strategy can adopt a centralized or distributed control to obtain the deviation compensation for the DC-bus voltage. The compensation is introduced into the droop-control equation to translate the droop curve. This method solves the problem of excessive bus-voltage deviation. However, when the droop curve is translated, the stability of the new operation point is not considered, and the working range of the converter is reduced. To solve these two problems, first, a DC microgrid model is established to analyze the stability of the system.

A. Simplified Modeling of DC Microgrid

An actual DC microgrid consists of many types, and establishing a unified model is difficult. To simplify the model, the present study makes the following hypotheses.

Hypothesis 1: the loads and intermittent sources with maximum power-point tracking are in a local load area. The common DC bus that connects them is considered as an ideal wire.

Hypothesis 2: the sources with droop control come from relatively remote areas such as wind power plant, PV power plant, energy-storage power station, and solid-state transformer. The line impedance cannot be ignored.

Hypothesis 3: the DC-bus current and branch currents also change in the same proportion during the dynamic process.

Since droop-control sources consist of many types and are easily influenced by the resources and weather, they require different droop curves to achieve reasonable load sharing. However, multiple converters may be present in the same

type, which can be considered as equivalent to one converter. The rated operation-point voltage of the equivalent converter is constant, and the droop coefficient becomes k/n, where n is the number of the converters in the same type of the source. We can obtain from hypothesis 3 that $\sum_{j=1}^{n} i_j / i_i = \mathrm{d}(\sum_{j=1}^{n} i_j)/\mathrm{d}i_i = k_i \sum_{i=1}^{n} k_i^{-1}$, where i_i and i_j are the output currents of source i and source j, respectively, k_i is the droop coefficient of source i. Thus, the equivalent circuit with n types of sources under a droop control is shown in Fig. 2.

$$\frac{\mathrm{d}i_i}{\mathrm{d}t} = \frac{1}{L_{\mathrm{d}i}}\left(V_{\mathrm{ref}i} - V_{\mathrm{bus}} - R_{\mathrm{d}i} i_i\right) \quad i = 1,2,\cdots,n \tag{1}$$

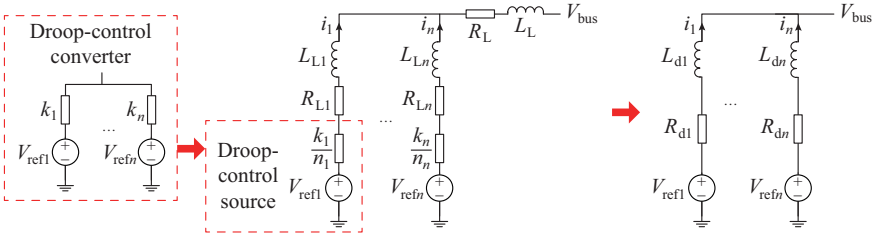

Fig. 2. Equivalent circuit with n types of sources under droop control.

Active loads and intermittent sources with the maximum power-point tracking are generally considered to run in a constant-power mode [27]. Therefore, in a local load area, all active loads and intermittent sources are equivalent to one constant power source, as expressed in (3).

$$\begin{cases} i(V_{\mathrm{bus}}) = \dfrac{P}{V_{\mathrm{bus}}} \\ P = \sum_{i=1}^{n} P_{\mathrm{L}i} - \sum_{i=1}^{n} P_{\mathrm{S}i} \end{cases} \tag{3}$$

where $P_{\mathrm{L}i}$ is the output power of the active load; and $P_{\mathrm{S}i}$ is the output power of the intermittent source with maximum power point tracking.

Similarly, the input capacitances of the constant-power sources and a bank of capacitors C_i connected to the bus are represented by a lumped capacitance, which is denoted as C. Similarly, the resistive loads R_i in the local load area are also lumped and denoted as R.

$$C = \sum_{i=1}^{n} C_i \tag{4}$$

$$R = \frac{1}{\sum_{i=1}^{n} \frac{1}{R_i}} \tag{5}$$

According to the above-mentioned results, the large-signal equivalent circuit of the DC microgrid is established, as shown in Fig. 3. Its mathematical model is expressed in (6).

$$\begin{cases} \dfrac{\mathrm{d}i_i}{\mathrm{d}t} = \dfrac{1}{L_{\mathrm{d}i}}\left(-R_{\mathrm{d}i} i_i + V_{\mathrm{ref}i} - V_{\mathrm{bus}}\right) \quad i = 1,2,\cdots,n \\ \dfrac{\mathrm{d}V_{\mathrm{bus}}}{\mathrm{d}t} = \dfrac{1}{C}\left(\sum_{i=1}^{n} i_i - \dfrac{V_{\mathrm{bus}}}{R} - \dfrac{P}{V_{\mathrm{bus}}}\right) \end{cases} \tag{6}$$

where $R_{\mathrm{d}i}$ and $L_{\mathrm{d}i}$ are the equivalent resistance and reactance of transmission line, respectively; $V_{\mathrm{ref}i}$ is the rated voltage of source i; and V_{bus} is the DC bus voltage.

$$\begin{cases} R_{\mathrm{d}i} = \dfrac{k_i}{n_i} + R_{\mathrm{L}i} + R_{\mathrm{L}} k_i \sum_{i=1}^{n} \dfrac{1}{k_i} & i = 1,2,\cdots,n \\ L_{\mathrm{d}i} = L_{\mathrm{L}i} + L_{\mathrm{L}} k_i \sum_{i=1}^{n} \dfrac{1}{k_i} & i = 1,2,\cdots,n \end{cases} \tag{2}$$

where $R_{\mathrm{L}i}$ and $L_{\mathrm{L}i}$ are the resistance and reactance of transmission line between source i and the DC bus, respectively; R_{L} and L_{L} are the resistance and reactance of the DC bus, respectively; and n_i is the number of the converters in the same type of source i.

We can obviously see that the model has a higher order, nonlinear, time-varying, and multivariable characteristic.

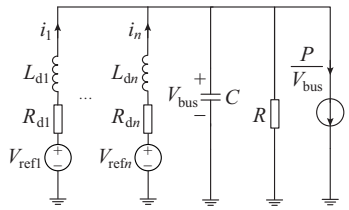

Fig. 3. Large-signal equivalent circuit of DC microgrid.

B. Small-signal Stability Analysis of DC Microgrid

To analyze the system stability, a Jacobian matrix is obtained from (6).

$$\boldsymbol{J} = \begin{bmatrix} -\dfrac{R_{\mathrm{d}1}}{L_{\mathrm{d}1}} & \cdots & 0 & \cdots & 0 & -\dfrac{1}{L_{\mathrm{d}1}} \\ \vdots & & \vdots & & \vdots & \vdots \\ 0 & \cdots & -\dfrac{R_{\mathrm{d}i}}{L_{\mathrm{d}i}} & \cdots & 0 & -\dfrac{1}{L_{\mathrm{d}i}} \\ \vdots & & \vdots & & \vdots & \vdots \\ 0 & \cdots & 0 & \cdots & -\dfrac{R_{\mathrm{d}n}}{L_{\mathrm{d}n}} & -\dfrac{1}{L_{\mathrm{d}n}} \\ \dfrac{1}{C} & \cdots & \dfrac{1}{C} & \cdots & \dfrac{1}{C} & -\dfrac{1}{C}\left(\dfrac{1}{R} - \dfrac{P}{V_{\mathrm{bus}}^2}\right) \end{bmatrix} \tag{7}$$

The characteristic equation is obtained from (7).

$$\frac{1}{C}\sum_{j=1}^{n}\left[\frac{1}{L_{\mathrm{d}j}}\prod_{i=1,i\neq j}^{n}\left(\lambda + \frac{R_{\mathrm{d}i}}{L_{\mathrm{d}i}}\right)\right] + \left(\lambda + \frac{1}{RC} - \frac{P}{CV_{\mathrm{bus}}^2}\right)\prod_{i=1}^{n}\left(\lambda + \frac{R_{\mathrm{d}i}}{L_{\mathrm{d}i}}\right) = 0 \tag{8}$$

Directly obtaining the $n+1$ eigenvalues is difficult. However, the stability only depends on the real part of these eigenvalues. We set $\lambda = a + bi$ and $M = P/V_{\text{bus}}^2$, and substitute them into (8).

$$\begin{cases} M = \displaystyle\sum_{j=1}^{n} \frac{a + \dfrac{R_{dj}}{L_{dj}}}{L_{dj}\left[\left(a + \dfrac{R_{dj}}{L_{dj}}\right)^2 + b^2\right]} + aC + \frac{1}{R} \\ 0 = b\left\{\displaystyle\sum_{j=1}^{n} \frac{-1}{L_{dj}\left[\left(a + \dfrac{R_{dj}}{L_{dj}}\right)^2 + b^2\right]} + C\right\} \end{cases} \tag{9}$$

According to the second formula in (9), these eigenvalues meet one of the following two conditions:

1) Condition 1: $b = 0$.

2) Condition 2: $\sum_{j=1}^{n} \{L_{dj}[(a + R_{dj}/L_{dj})^2 + b^2]\}^{-1} = C$.

When Condition 1 is met, these eigenvalues are real roots. Condition 1 is then substituted into the first formula in (9).

$$M = \sum_{j=1}^{n} \frac{1}{L_{dj}a + R_{dj}} + aC + \frac{1}{R} \tag{10}$$

Figure 4 shows the relationship between M and a under the Condition 1. The positive root depends on the eigenvalues in $[-\min_{j=1,2,\ldots,n}(R_{dj}/L_{dj}), +\infty]$. Some eigenvalues gradually move to the right-half plane with the increase of M. When the eigenvalue appears positive, the system is unstable.

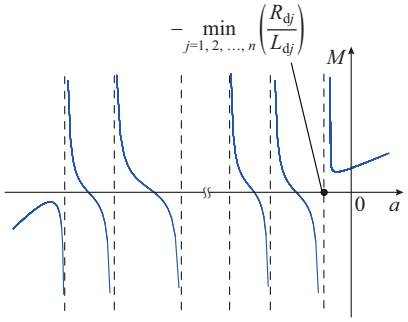

Fig. 4. Relationship between M and a under Condition 1.

When Condition 2 is met, the derivative of the first formula in (9) is taken, and Condition 2 is substituted.

$$\frac{dM}{da} = \sum_{j=1}^{n} \frac{2b^2}{L_{dj}\left[\left(a + \dfrac{R_{dj}}{L_{dj}}\right)^2 + b^2\right]^2} > 0 \tag{11}$$

By combining the two cases, we learn that when the droop curves and circuit parameters do not change, the increase in M will deteriorate the stability of the DC microgrid. Considering a steady state, the differential terms in (6) becomes zero, and (6) degenerates into a series of algebraic equations.

$$\begin{cases} i_i = \dfrac{V_{refi} - V_{\text{bus}}}{R_{di}} \quad i = 1,2,\cdots,n \\ \displaystyle\sum_{i=1}^{n} i_i = \frac{V_{\text{bus}}}{R} + \frac{P}{V_{\text{bus}}} \end{cases} \tag{12}$$

M is further calculated according to (13).

$$M = \sum_{i=1}^{n} \frac{\dfrac{V_{refi}}{V_{\text{bus}}} - 1}{R_{di}} - \frac{1}{R} \tag{13}$$

From (13), when the droop curves and circuit parameters do not change, M is only determined by the DC-bus voltage. Thus, when the droop curves and circuit parameters do not change, the stability of the DC microgrid becomes worst at the maximum point of M (the lowest limit of the DC-bus voltage). Hence, when the stability of the droop curve is determined, we can only consider the lowest point in this droop curve.

III. Multi-objective Optimization Segmented Droop Control Strategy

In the conventional droop control, when the rated operation point changes, the droop curves move in parallel to cross the new rated operation point. Figure 5 shows the droop curves used in an energy-storage power source. C', C'' and C''' represent the rated operation points of the source, and the current is expressed in the per-unit value. A and E represent the maximum output and input power of the source, respectively. V_{high} and V_{low} are the highest voltage and lowest voltage in the controllable range, respectively. I_{high} and I_{low} are the maximum current and minimum current in the controllable range, respectively.

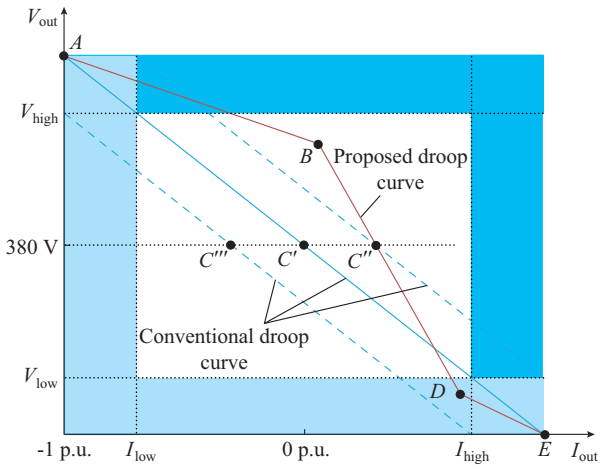

Fig. 5. Droop curves under different droop controls.

In [3], [19], and [20], a secondary control is added, which makes the droop curve to shift, and the rated operation point moves from C' to C'' or C'''. These control methods narrow the scope of the droop control. The working range under the conventional droop control does not include the yellow or orange area. Moreover, when the droop curve is translated, the stability of the system is not determined. The farther the rat-

ed operation point is from the zero point, the narrower is the working range. The source easily exits the droop control, which is not conducive to the controllable operation of the DC microgrid.

To address this problem, a multi-objective optimization segmented droop control is proposed in this paper, as shown by the red line in Fig. 5. The droop curve is divided into three segments from A to E. The middle segment crosses the rated operation point C''. The droop coefficient of the converter is changed in points B and D. Thus, the droop control can cover the whole operation range. The droop coefficient of the source at different rated operation points is obviously not fixed any more. Therefore, we need to consider some control objectives and stable constraints to obtain a new curve.

A. Objective Functions

The line resistance is usually dynamic and difficult to accurately measure. Thus, minimizing the effect of the line resistance on the real-time power distribution is necessary. As the sources mainly operate in the BD segment, this study reduces the effect of the line resistance by increasing its droop coefficient based on (1). However, the oversized droop coefficient in AB and DE will lead to very quick deviation from the rated operation point. Thus, the first objective function is expressed in (14).

$$f_1 = \sum_{i=1}^{N}\left(\frac{1}{k_{iBD}} + k_{iAB} + k_{iDE}\right) \tag{14}$$

where N is the number of sources; and k_{iAB}, k_{iBD}, and k_{iDE} are the droop coefficients of segments AB, BD and DE of the proposed droop curve, respectively.

To ensure that the output/input power of each source match its corresponding capacity, the droop coefficient of each segment should be proportional to its capacity. Thus, the second objective function is obtained.

$$f_2 = \sum_{i=1}^{N}\left|\frac{k_{iAB}}{S_i} - \bar{k}_{AB}\right| + \sum_{i=1}^{N}\left|\frac{k_{iBD}}{S_i} - \bar{k}_{BD}\right| + \sum_{i=1}^{N}\left|\frac{k_{iDE}}{S_i} - \bar{k}_{DE}\right| \tag{15}$$

$$\begin{cases} \bar{k}_{AB} = \dfrac{1}{N}\displaystyle\sum_{i=1}^{N}\frac{k_{iAB}}{S_i} \\ \bar{k}_{BD} = \dfrac{1}{N}\displaystyle\sum_{i=1}^{N}\frac{k_{iBD}}{S_i} \\ \bar{k}_{DE} = \dfrac{1}{N}\displaystyle\sum_{i=1}^{N}\frac{k_{iDE}}{S_i} \end{cases} \tag{16}$$

where S_i is the capacity of source i.

To determine whether the two objective functions are in the same direction or not, the validation is performed. Figure 6 shows that when a group of droop coefficients are changed, the two objective functions obviously have different directions of change and cannot be simplified as an objective function.

B. Stability Constraints

The DC microgrid must satisfy the stability throughout the entire operation range. However, numerous operation points exist on a droop curve. Therefore, determining the stability of each operation point is not feasible. According to the relevant conclusions from Section II, when the droop curves and circuit parameters do not change, the stability can be determined at the point of maximum M (or the lowest DC-bus voltage) in the same segment of the droop curve, i.e., at B, D, and E in the proposed droop curve. The droop curve of each source may be different, and B, D, and E in all droop curves need to be determined, as expressed in (17).

$$\begin{cases} eig_i\left(\boldsymbol{J}_{Bj}\right) < 0 \\ eig_i\left(\boldsymbol{J}_{Dj}\right) < 0 \\ eig_i\left(\boldsymbol{J}_{Ej}\right) < 0 \end{cases} \tag{17}$$

where $i = 1,2,...,n+1$; $j = 1,2,...,n$; $\boldsymbol{J}_{Bj}$, $\boldsymbol{J}_{Dj}$, and $\boldsymbol{J}_{Ej}$ represent the Jacobian matrices at B, D, and E of the j^{th} source, respectively; and $eig_i(\cdot)$ represents the real part of the eigenvalues of the Jacobian matrix.

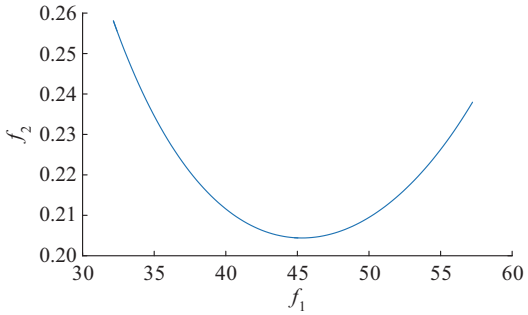

Fig. 6. Relationship between two objective functions.

C. Implementation of Proposed Droop Control

The realization of the proposed droop control is shown in Fig. 7.

After the translation of all droop-control converters, $\Delta U_{\text{dc}i}$ and the parameters of the DC microgrid are sent to NSGA-II for calculation. B and D of each source are searched by NSGA-II, as shown in Fig. 8, where n_{c} and $n_{\text{c,max}}$ are the cycle time and the maximum cycle time, respectively. The droop curves of several converters are simultaneously calculated. The equipment layer determines the droop coefficient of the converter by detecting the voltage or current. Finally, the droop curves are sent to the corresponding converters. However, when the new rated operation point of the source is too close to the droop-control boundary, a case may exist in which the three segments cannot satisfy the stability constraints because the operation range is relatively small. At this time, conventional droop control is used instead of the proposed droop control. Then, the central controller sends the droop curves to the local controllers, and a low bandwidth-timing communication network will be used. The local controller determines the working droop segment by detecting the current. The converter is controlled based on the double closed loops.

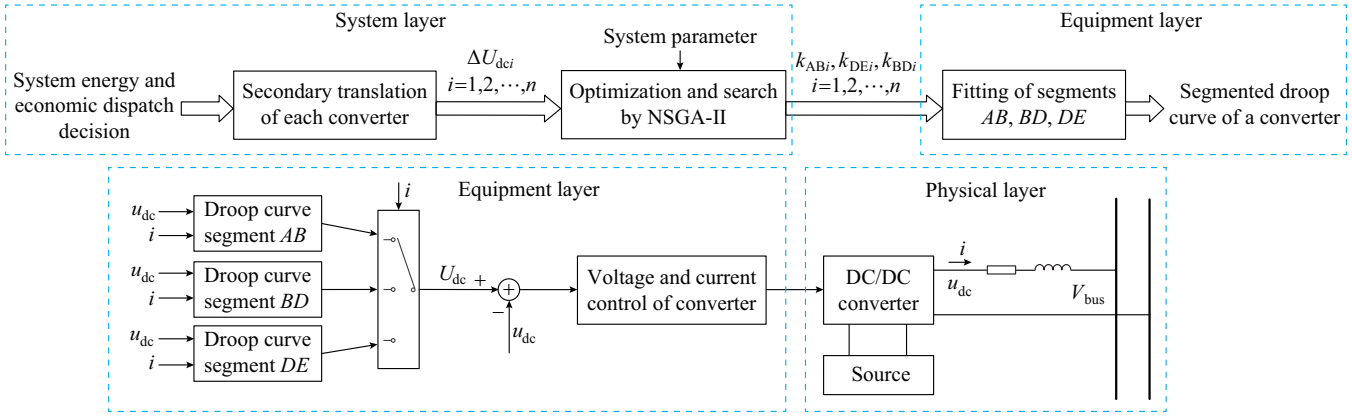

Fig. 7. Realization of proposed droop control.

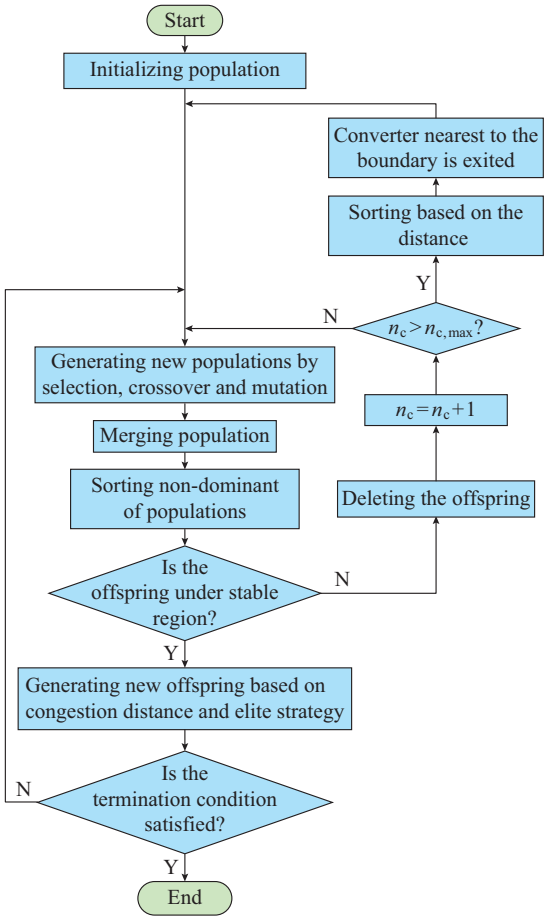

Fig. 8. Flowchart of NSGA-II.

IV. Real-time Simulation Verification

To verify the multi-objective optimization segmented droop control, the DC microgrid system is built in RT-Lab, as shown in Fig. 9. Converter 1 (38 kVA) and converter 2 (76 kVA) are droop-control converters. The other side of Converter 1 is connected to a 20 kV DC grid, and that of Converter 2 is connected to a 72 V battery pack.

Their rated operation point voltage is 380 V. Converter 3 is a PV converter with the maximum power-point tracking, and Converter 4 is a constant-power load. The input capacitances of the two converters are both 2 mF.

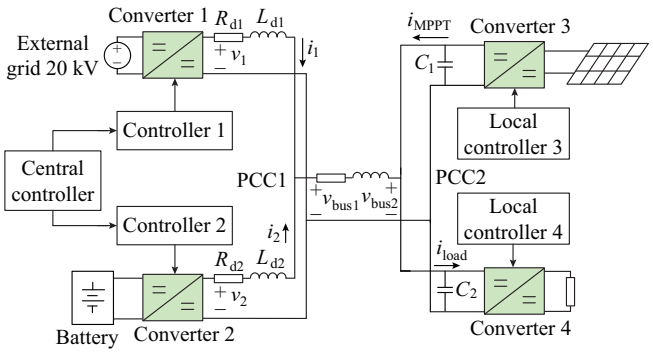

Fig. 9. Simulation circuit of DC microgrid.

The line impedances are as follows: L_{d1} = 0.4 mH, L_{d2} = 0.3 mH, L_{d3} = 0.5 mH, R_{d1} = 40 mΩ, R_{d2} = 35 mΩ, R_{d3} = 90 mΩ. The rated operation points and load cases are listed in Table I. We assume that the load prediction is accurate at each economic dispatch in the system layer. Considering the different cases, NSGA-II is used to calculate the optimal droop curves. The search processes for Cases 1-3 are shown in Fig. 10, where the blue droop curves represent the searched droop curves of all generations, and the red droop curves represent the optimal droop curves. The search processes of the two objective functions under Case 1 are shown in Fig. 11(d). After 150 generations of evolution, the two target functions reach the numerical value of relative stability. The evolution is terminated after the 350th generation, and the final droop curves are obtained.

TABLE I
Rated Operation Points and Load Cases

Source	Rated current (A)			
	Case 1	Case 2	Case 3	Case 4
Converter 1	35	45	30	45
Converter 2	20	28	17	80
Converter 3	15	19	17	18
Converter 4	75	92	61	133

The optimal droop curves are sent from the central controller to the corresponding converters. The reference value of the converter voltage is calculated according to the opti-

mal droop curve and output current, as shown in Fig. 7. The output current also determines which segment of the optimal droop curve is selected as a working curve. The voltages and currents of the DC microgrid are shown in Fig. 11(a), (b), where v_1 and v_2 are the output voltages of Converters 1 and 2, respectively, v_{bus1} and v_{bus2} are the DC-bus voltages at point of common coupling (PCC) 1 and PCC 2, respectively, i_{MPPT} is the output current of Converter 3, and i_{load} is the current of load. The droop coefficients of Converters 1 and 2 in different cases are shown in Fig. 11(c).

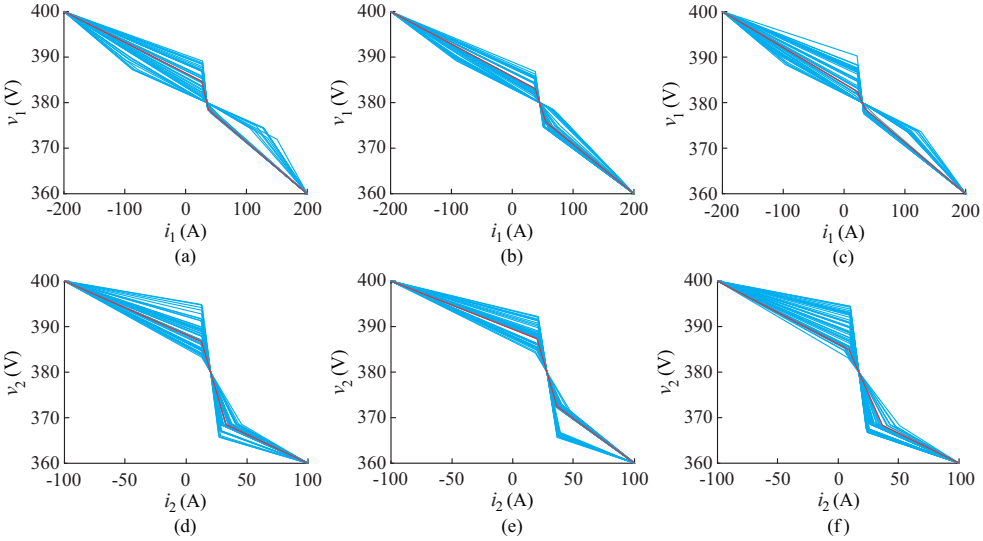

Fig. 10. Search processes of droop curves in Cases 1-3. (a) Converter 1 in Case 1. (b) Converter 1 in Case 2. (c) Converter 1 in Case 3. (d) Converter 2 in Case 1. (e) Converter 2 in Case 2. (f) Converter 2 in Case 3.

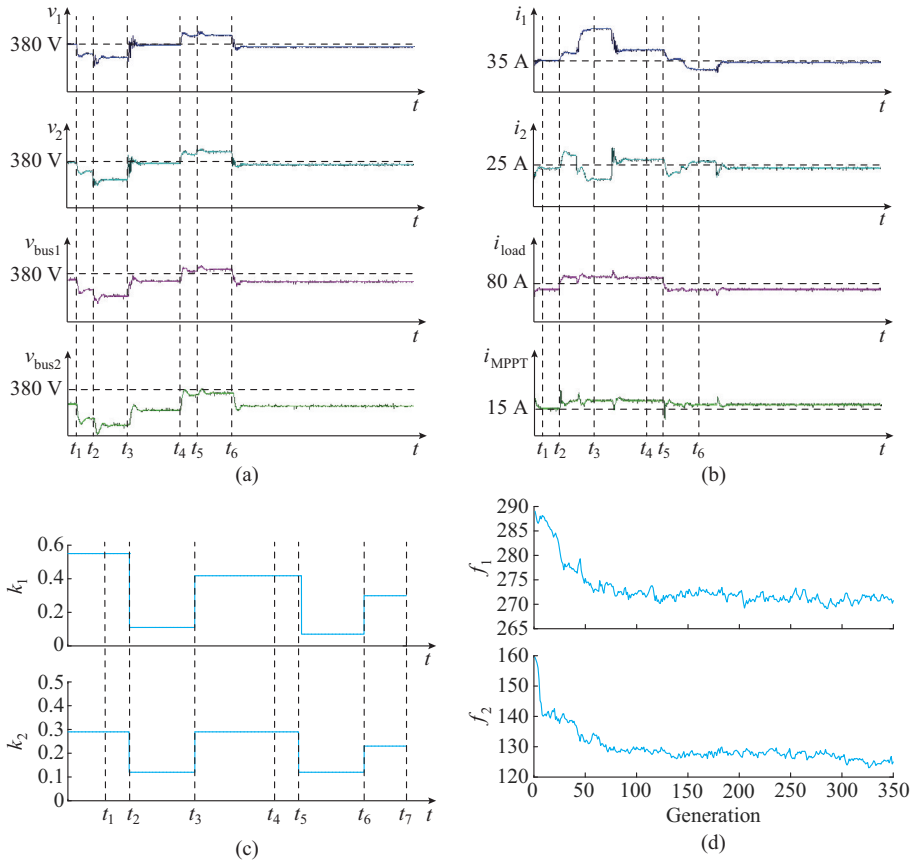

Fig. 11. Simulation results. (a) Voltages of DC microgrid. (b) Currents of DC microgrid. (c) Droop coefficients at different time. (d) Search processes of two objective functions in Case 1.

From t_0 to t_1, all converters work in Case 1. Converters 1 and 2 work at the rated operation points of the droop curves shown in Fig. 10(a) and (d). We can observe that output voltages v_1 and v_2 of Converters 1 and 2, respectively, approach

380 V. Because of the existence of line loss, v_{bus1} and v_{bus2} are slightly less than 380 V. At t_1, Converters 3 and 4 transform to Case 2, whereas the new droop curves are not calculated at the central controller. Further, Converters 1 and 2 still use the droop curves shown in Fig. 10(a) and (d). At t_1, the load increases from 1 to 2 kW, the output voltages of Converters 1 and 2 decrease, and the output currents increase. While waiting for the end of the transient process, at t_2, the operation points of Converters 1 and 2 shift from the middle to the bottom segment according to the output currents.

At t_3, the new droop curves are calculated at the central controller, and Converters 1 and 2 use the droop curves shown in Fig. 10(b) and (e). All converters work in Case 2. Converters 1 and 2 work again at the rated operation points, and output voltages v_1 and v_2 approach back to 380 V. The droop coefficients correspondingly change at this time, as shown in Fig. 11(c).

At t_4, Converters 3 and 4 change from Case 2 to Case 3, and the droop curves of Converters 1 and 2 remain unchanged. Since the load is reduced, the output voltages of Converters 1 and 2 increase and the output currents decrease. While waiting for the end of the transient process, at t_5, the operation points of Converters 1 and 2 shift from the middle to the top segment, as shown in Fig. 10(b) and (e), according to the output currents.

At t_6, the new droop curves are calculated again at the central controller, and Converters 1 and 2 use the droop curves shown in Fig. 10(c) and (f). All converters work in Case 3. Converters 1 and 2 work again at the rated operation points in the middle segment, and output voltages v_{out1} and v_{out2} approach back to 380 V. The droop coefficients correspondingly change again at this time.

However, when all converters work in Case 4, the rated operation point of Converter 2 is too close to the droop-control boundary. The proposed droop curve of Converter 2 cannot satisfy the requirements of stability. Thus, a conventional droop curve is used. The search processes for the droop curves are shown in Fig. 12, where the blue droop curves represent the searched droop curves of all generations, and the red curves represent the final droop curves.

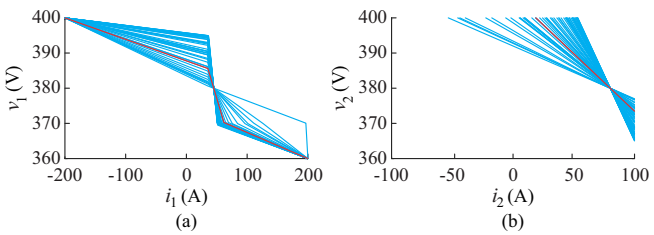

Fig. 12. Search processes of droop curves in Case 4.

In the above-mentioned processes, the DC microgrid retains good stability, thus the stability conclusion and the effectiveness of the proposed droop control are supported.

V. Conclusion

A simplified model of a typical DC microgrid is first built in this study, and the Jacobian matrix is used to analyze the system stability. When the droop curves and circuit parameters do not change, the stability of the DC microgrid is the worst at the lowest DC-bus voltage. Therefore, when the droop control effect on the system stability is determined, we only need to consider the lowest point of the voltage in the droop curve. Thus, a huge computation work in determining the system stability at all operation points in a droop curve is avoided. Second, to ensure that the droop control source can work efficiently in the droop control in the whole operation range, a multi-objective optimization segmented droop control is proposed. The optimization objectives, including the influence of eliminating the line resistance and capacity matching, are considered in the search process. The constraints are the stability at the *B*, *D*, and *E* points in the droop curves. When the rated operation points are changed by the economic dispatch in the system layer, the multi-objective optimization segmented droop control solves the problem in which the droop control range does not always match the operation range. Continuous droop control in a larger range of operation is realized. Finally, a DC microgrid simulation model with two droop-control sources is built on RT-Lab. The simulation results in four cases are provided to prove that the stability conclusion and the proposed droop control are valid.

References

[1] H. Lotfi and A. Khodaei, "AC versus DC microgrid planning," *IEEE Transactions on Smart Grid*, vol. 8, no. 1, pp. 296-304, Aug. 2015.

[2] M. K. Zadeh, R. Gavagsaz-Ghoachani, S. Pierfederici *et al.*, "Stability analysis and dynamic performance evaluation of a power electronics-based DC distribution system with active stabilizer," *IEEE Journal of Emerging & Selected Topics in Power Electronics*, vol. 4, no. 1, pp. 93-102, Jan. 2016.

[3] X. Yu, X. She, X. Ni *et al.*, "System integration and hierarchical power management strategy for a solid-state transformer interfaced microgrid system," *IEEE Transactions on Power Electronics*, vol. 29, no. 8, pp. 4414-4425, Aug. 2014.

[4] T. Dragičević, J. M. Guerrero, J. C. Vasquez *et al.*, "Supervisory control of an adaptive-droop regulated DC microgrid with battery management capability," *IEEE Transactions on Power Electronics*, vol. 29, no. 2, pp. 695-706, Feb. 2014.

[5] A. Bidram, A. Davoudi, F. L. Lewis *et al.*, "Secondary control of microgrids based on distributed cooperative control of multi-agent systems," *IET Generation Transmission & Distribution*, vol. 7, no. 8, pp. 822-831, Aug. 2013.

[6] J. Xiao, P. Wang, and L. Setyawan, "Multilevel energy management system for hybridization of energy storages in DC microgrids," *IEEE Transactions on Smart Grid*, vol. 7, no. 2, pp. 847-856, Mar. 2016.

[7] I. U. Nutkani, P. C. Loh, P. Wang *et al.*, "Decentralized economic dispatch scheme with online power reserve for microgrids," *IEEE Transactions on Smart Grid*, vol. 8, no. 1, pp. 139-148, Aug. 2017.

[8] A. Tah and D. Das, "An enhanced droop control method for accurate load sharing and voltage improvement of isolated and interconnected DC microgrids," *IEEE Transactions on Sustainable Energy*, vol. 7, no. 3, pp. 1194-1204, Jul. 2016.

[9] A. Huang, M. L. Crow, G. T. Heydt *et al.*, "The future renewable electric energy delivery and management (FREEDM) system: the energy internet," *Proceedings of the IEEE*, vol. 99, no. 1, pp. 133-148, Feb. 2011.

[10] C. Chen, S. Duan, T. Cai *et al.*, "Smart energy management system for optimal microgrid economic operation," *IET Renewable Power Generation*, vol. 5, no. 3, pp. 258-267, Jun. 2011.

[11] M. Nemati, K. Bennimar, S. Tenbohlen *et al.*, "Optimization of microgrids short term operation based on an enhanced genetic algorithm," in *Proceedings of the PowerTech*, Eindhoven, the Netherlands, Jun.-Jul. 2015, pp. 1-6.

[12] C. Marnay, G. Venkataramanan, M. Stadler *et al.*, "Optimal technolo-

gy selection and operation of commercial-building microgrids," *IEEE Transactions on Power Systems*, vol. 23, no. 3, pp. 975-982, Sept. 2008.
[13] E. Sortomme and M. A. El-Sharkawi, "Optimal power flow for a system of microgrids with controllable loads and battery storage," in *Proceedings of the IEEE PES Power Systems Conference and Exposition*, Seattle, USA, Mar. 2009, pp. 1-5.
[14] S. Chakraborty, M. D. Weiss, and M. G. Simoes, "Distributed intelligent energy management system for a single-phase high-frequency AC microgrid," *IEEE Transactions on Industrial Electronics*, vol. 54, no. 1, pp. 97-109, Mar. 2007.
[15] J. M. Guerrero, J. C. Vasquez, J. Matas *et al*., "Hierarchical control of droop-controlled AC and DC microgrids – a general approach toward standardization," *IEEE Transactions on Industrial Electronics*, vol. 58, no. 1, pp. 158-172, Jan. 2011.
[16] J. Schonbergerschonberger, R. Duke, and S. D. Round, "DC-bus signaling: a distributed control strategy for a hybrid renewable nanogrid," *IEEE Transactions on Industrial Electronics*, vol. 53, no. 5, pp. 1453-1460, Oct. 2006.
[17] B. T. Irving and M. M. Jovanovic, "Analysis, design, and performance evaluation of droop current-sharing method," in *Proceedings of 15th Annual IEEE Applied Power Electronics Conference and Exposition*, New Orleans, USA, Feb. 2000, pp. 235-241.
[18] X. Yu, X. She, X. Zhou *et al*., "Power management for DC microgrid enabled by solid-state transformer," *IEEE Transactions on Smart Grid*, vol. 5, no. 2, pp. 954-965, Mar. 2014.
[19] X. Lu, J. M. Guerrero, K. Sun *et al*., "An improved droop control method for DC microgrids based on low bandwidth communication with DC bus voltage restoration and enhanced current sharing accuracy," *IEEE Transactions on Power Electronics*, vol. 29, no. 4, pp. 1800-1812, Jan. 2013.
[20] P. Wang, X. Lu, X. Yang *et al*., "An improved distributed secondary control method for DC microgrids with enhanced dynamic current sharing performance," *IEEE Transactions on Power Electronics*, vol. 31, no. 9, pp. 6658-6673, Jan. 2016.
[21] S. R. Reddy, *Fundamentals of Power Electronics*, Boca Raton, USA: CRC Press, 2000, pp. 187-263.
[22] J. Sun, "Impedance-based stability criterion for grid-connected inverters," *IEEE Transactions on Power Electronics*, vol. 26, no. 11, pp. 3075-3078, Dec. 2011.
[23] F. Liu, J. Liu, H. Zhang *et al*., "Generalized stability criterion for multi-module distributed DC system," *Journal of Power Electronics*, vol. 14, no. 1, pp. 416-421, Jun. 2014.
[24] W. Du, J. Zhang, Y. Zhang *et al*., "Stability criterion for cascaded system with constant power load," *IEEE Transactions on Power Electronics*, vol. 28, no. 4, pp. 1843-1851, Apr. 2013.
[25] H. J. Kim, S. W. Kang, G. S. Seo *et al*., "Large-signal stability analysis of DC power system with shunt active damper," *IEEE Transactions on Industrial Electronics*, vol. 63, no. 10, pp. 6270-6280, Oct. 2016.
[26] M. K. Zadeh, R. Gavagsaz-Ghoachani, J. P. Martin *et al*., "Discrete-time tool for stability analysis of DC power electronics-based cascaded systems," *IEEE Transactions on Power Electronics*, vol. 32, no. 1, pp. 652-667, Jan. 2017.
[27] A. P. N. Tahim, D. J. Pagano, E. Lenz *et al*., "Modeling and stability analysis of islanded DC microgrids under droop control," *IEEE Transactions on Power Electronics*, vol. 30, no. 8, pp. 4597-4607, Aug. 2015.
[28] N. Ghanbari, P. M. Shabestari, A. Mehrizi-Sani *et al*., "State-space modeling and reachability analysis for a DC microgrid," in *Proceedings of Applied Power Electronics Conference and Exposition (APEC)*, Anaheim, USA, Aug. 2018, pp. 1-8.
[29] J. Bu, M. Zhou, X. Lan *et al*., "Optimization for airgap flux density waveform of flywheel motor using NSGA-2 and kriging model based on MaxPro design," *IEEE Transactions on Magnetics*, vol. 53, no. 8, pp. 1-6, Aug. 2017.

Haiyuan Liu received the B. S. degree from Sichuan Normal University, Chengdu, China, in 2001, and the M.S. degree from the China University of Mining and Technology, Xuzhou, China, in 2006, where she is presently working towards her Ph.D. degree. She is also working as a teacher in the School of Mathematics, China University of Mining and Technology, Xuzhou, China. Her current research interests include intelligent control theory and its application.

Yingjie Wang received the B. S. degree in mechanical engineering from Central South University, Changsha, China, in 2001 and the Ph.D. degree in electrical engineering from the China University of Mining and Technology, Xuzhou, China, in 2012. He is presently working as an associate professor in the School of Electrical and Power Engineering, China University of Mining and Technology, Xuzhou, China. His current research interests include power quality, microgrids and medium-voltage AC drives.

Min Wang received the B.S. degree in electrical engineering from the Jiangxi University of Science and Technology, Ganzhou, China, in 2017. He is currently working toward the M.S. degree in electrical engineering with the China University of Mining and Technology, Xuzhou, China. His current research interests include power quality and microgrids.

Yinan Guo received the Ph. D. degree in control theory and control engineering from the China University of Mining and Technology, Xuzhou, China, in 2003. She is presently working as a professor in the School of Information and Control Engineering, China University of Mining and Technology, Xuzhou, China. Her current research interests include computation intelligence, imbalance learning and control theory.

Jiashi Wang received the M. S. degree in electrical engineering from the China University of Mining and Technology, Xuzhou, China, in 2017. He is currently working toward the Ph.D. degree in electrical engineering with the Shanghai Jiao Tong University, Shanghai, China. His current research interests include grid emulator and converter control design.

Gang Shen received the Ph. D. degree in mechanical engineering from the Harbin Institute of Technology, Harbin, China, in 2011. He is presently working as a professor in the School of Mechanical Engineering, China University of Mining and Technology, Xuzhou, China. His current research interests include redundant drive electro-hydraulic servo system and parallel mechanism.

Guoqiang Liao received the B. S. degree in traffic engineering from the East China Jiaotong University, Nanchang, China, in 2002. Nowadays, he is a senior engineer in CRRC Zhuzhou Locomotive Co., Ltd., Zhuzhou, China.